A P-band Radar Mission to Mars

Bruce Campbell (Member, IEEE)
Center for Earth and Planetary Studies
Smithsonian Institution
PO Box 37012, Washington, DC 20003-7012
202-633-2472
campbellb@nasm.si.edu

Anthony Freeman (Fellow, IEEE), Louise Veilleux, Brian Huneycutt, Michael Jones, Robert Shotwell
Jet Propulsion Laboratory
4800 Oak Grove Drive
Pasadena, CA 91109

Abstract- Large regions of Mars are covered by dust that obscures geological evidence for fluvial channels, the extent of volcanic flows, and features associated with near-surface ground ice. We describe a Mars orbiting mission carrying a P-band SAR to map these hidden surface features. Mapping would be carried out in HH and VV polarizations, with the comparison of the two expected to yield a distinction between surface echoes and subsurface features beneath up to 5 m of dust. Repeat-pass interferometry data would also be collected to characterize volatile migration at the poles, aeolian shifting of the dust mantle, and possible volcanic deformation. This paper describes the technical design of a P-band SAR for global mapping of Mars, and the characteristics of the proposed mission.

1. INTRODUCTION

The surface of Mars retains a geologic record of the planet's climate, which has changed dramatically over time. Older highland regions are scarred by impact craters and basins that date to the end of the "late heavy bombardment". Younger features reveal the influence of flowing water during early martian history, and the possibly longer-lived role of effusive volcanic events. Recent orbital observations suggest that volcanic eruptions and surface discharge of water may continue, at very low levels, to the present.

Up to one-third of the martian surface is obscured by layers of dust deposited by aeolian processes [1]. Ash and sedimentary deposits, produced by volcanoes and flowing water, can be quite thick, but wind-blown dust deposits are likely on the order of meters in depth. Beneath these mantling deposits are geologic features of considerable importance in deciphering the record of climate change on Mars, and identifying locations that may harbor evidence of past or present life.

Current remote sensing instruments can reveal only the upper few cm of mantling materials, primarily through measurement of thermal infrared signatures. Radar sounding at wavelengths greater than 15 m, to be carried out by the MARSIS and SHARAD orbital instruments, will study sub-surface layers at depths greater than 100 m. There are no current or planned observations that will characterize the nature of the upper ~10 m of the near-surface environment. This is a crucial gap in the global reconnaissance of Mars, since the upper 10-m region is most accessible for drilling and sampling.

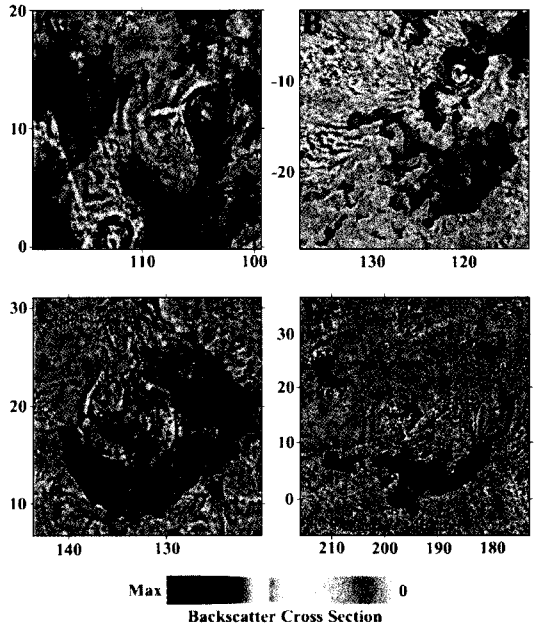

Figure 1. Arecibo 12.6-cm radar measurements of Mars [2], showing higher backscatter from rough volcanic materials surrounding the Tharsis volcanoes (a-c) and within a channel in Elysium (d). These rugged surfaces are covered by dust with depth of 10's of cm or more.

Synthetic-aperture radar (SAR), particularly at longer wavelengths, can be used to obtain information on sub-surface properties and map buried features. Earth-based radar mapping of Mars, even at 12.6-cm wavelength and

relatively low (10's of km) spatial resolution, shows that sub-surface rough terrain can be detected (Figure 1). The martian dust is clearly not too deep or lossy to permit effective radar penetration [2,3].

To address the need for near-surface probing of Mars, we proposed a NASA Scout mission called "Eagle" in 2002. This mission concept centers on a modified Odyssey spacecraft, carrying a 6-m deployable antenna and a 60-cm (P-band) imaging radar system. In the following sections, we present the scientific rationale for our selection of SAR operating parameters, examples of comparable terrestrial and planetary data, the technical design of the Eagle radar, and an overview of the mission design and operations.

2. SAR System Parameters

The current "state of the art" in imaging radar systems is represented by multi-wavelength, fully polarimetric sensors like the NASA/JPL AIRSAR or the Shuttle-borne Space Radar Laboratory (or SIR-C). While such a sensor might be feasible for Mars within the scope of a "line" mission such as the Mars Reconnaissance Orbiter, we emphasize here that important science can be obtained under the constraints of a Scout-class mission. The principal limit under such a program is overall cost, which forces careful choices in instrument complexity and mission operations. In this section, we detail the rationale for our choice of a single-frequency, dual-polarization radar system for Eagle.

Our initial goal is to obtain global radar image coverage of Mars at ~100 m spatial resolution (comparable to Magellan data for Venus), with higher-resolution (~30 m) imaging of interesting sites. Limiting the area of interest to regional mapping would assume that we fully understand the near-surface of Mars, and risks missing important, unexpected features. We also specified a one Earth-year operating period for the mission, which defines the total possible returned data volume.

The choice of radar wavelength, λ, is a compromise between depth of penetration and detection of sub-surface features. The depth of penetration increases with λ, but most natural surfaces also tend to appear "smoother" as the incident wavelength increases. Since we depend upon diffuse scattering from buried features to map the sub-surface, the incident wavelength cannot be increased without bound. Based on experience with lunar and terrestrial radar observations, P-band signals offer an excellent balance of penetration and scattering properties.

The polarization choice for Eagle is guided by the desire to (a) maximize penetration and (b) constrain the proportion of radar signal that arises from sub-surface scattering. The first criterion dictates a V-polarized transmit and receive state (VV), since the Fresnel coefficients for a dielectric surface permit the highest degree of transmission in this configuration. Circularly-polarized signals, with one-half of the incident power in the horizontally (H) polarized state, will not be as effective for sub-surface probing. The second criterion may be addressed with measurements of backscatter in the HH polarization mode.

The ratio of HH- to VV-polarized backscatter coefficient is the most direct indicator of the effects of a surface dielectric interface. In the most general case, the role of sub-surface scattering is convolved with the dielectric constant of this surface interface. For Mars dust, we may safely assume a real dielectric constant, $\varepsilon\varepsilon$, dominated by density (as observed for the lunar regolith and dry terrestrial rock powders) [4]. In this case, the range of $\varepsilon\varepsilon$ is plausibly 2.5-3.0. We may also constrain the expected polarization behavior of surface and sub-surface rough interfaces, using comparisons of AIRSAR and terrestrial field data. With these constraints, it is possible to use the HH/VV ratio as a guide to the fraction of sub-surface echo.

The incidence angle for radar measurements is likewise a compromise between competing factors. Lower incidence angles (closer to the nadir direction) provide greater backscatter power from any given surface, but also reduce the polarization differences due to Fresnel transmission through a mantling interface. Higher incidence angles lead to lower signal strength. We determined that 35-40° is the best operating range for a Mars orbital imaging radar.

How deep might a P-band, VV-polarized Mars SAR penetrate? The major unknown is the loss tangent, $\tan\delta$, of the martian near-surface layers. The loss tangent of dry materials at microwave frequencies is largely dictated the bulk chemistry, and specifically by the abundance of "lossy" minerals such as hematite or ilmenite. Our best guide for the possible range of loss tangents is that of the Apollo lunar samples, for which $\tan\delta$ extends from ~0.001 (highland rocks) to ~0.04 (high-titanium basalts) [4]. Given the penetration observed at S-band in Arecibo data (Figure 1), assumption of much higher loss tangents does not seem warranted.

Figure 2 shows the "detection depth" for a moderately rough rock surface buried by a dust layer. We have assumed a system noise floor for the backscatter coefficient, σ^0, of -35 dB, and a detection threshold 3 dB above this floor. The shaded area shows the range of $\tan\delta$ for which we can detect the buried rough surface beneath 5 m of dust. Rougher terrain could be detected at greater depths. Even for quite lossy mantling deposits, penetration depths of 3 m are feasible.

In summary, our trade studies of SAR operating parameters show that a high science return is possible using a P-band system capable of making observations in VV and HH polarization. Penetration depths of 3-5 m in martian dust are achievable by such a radar.

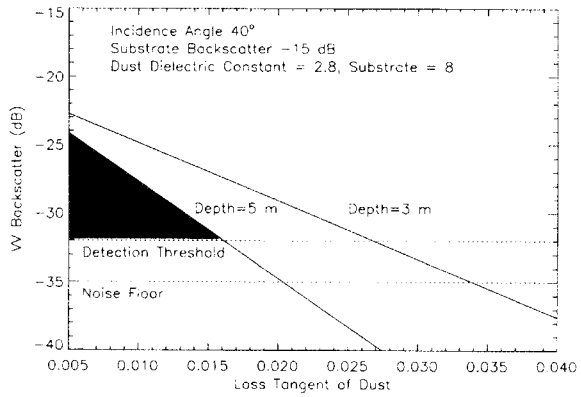

Figure 2. VV-polarization backscatter coefficient of a buried rough lava flow as a function of mantling deposit loss tangent. Shaded region shows the range of loss tangent for which we may detect this buried terrain at 5 m depth.

3. Terrestrial and Planetary Radar Studies

P-band radar observations have "heritage" in both terrestrial and planetary remote sensing. In this section, we present examples of ongoing studies that apply long-wavelength observations to Mars-analog environments.

The most obvious application of a Mars-orbital imaging radar is the detection and mapping of fluvial features beneath the dust. In particular, radar mapping could reveal small stream channels and gully features that are muted or buried by aeolian deposits. These buried features may play a key role in identifying areas of recent water discharge, which are good targets for the search for past and present life. The three Shuttle-borne imaging radar experiments showed the value of deep radar probing when they revealed the existence and extent of a trans-African drainage system that permitted human settlement in areas now covered by sand sheets (Figure 3). Penetration depths for L-band signals are on the order of 1-2 m, with radar-dark regions representing deep sand, lossy materials, or smooth buried terrain [5, 6].

Ground ice on Mars is also of considerable interest for radar probing. Orbital neutron spectrometer measurements strongly suggest that large quantities of water are present in the upper meter of the martian crust at high latitudes [7]. Constraining the physical boundaries of ground-ice deposits, and identifying large masses of relatively "clean" ice near the surface, could be accomplished by orbital radar mapping. The former goal would rely on finding diagnostic differences in the surface or volume-scattering properties of martian "permafrost" relative to other terrain. The second goal is more unambiguously addressed, since it is known that ice masses with moderate abundances of suspended rocks or internal cracks exhibit strong radar backscatter enhancement and distinctive polarization ratios.

This type of radar scattering behavior for ices has been observed for terrestrial ice sheets, the polar caps of Mars, the icy Galilean satellites of Jupiter, and ice deposits in permanently shaded craters on Mercury [8, 9, 10, 11, 12]. Recent 70-cm Arecibo radar images, with spatial resolution of 300-400 m, of the Moon's poles revealed no similar signatures (Figure 4) [13]. A very "dirty" martian ice deposit, analogous to terrestrial permafrost, would not have a strong coherent return, but Eagle could detect dust-covered ice masses if they exist.

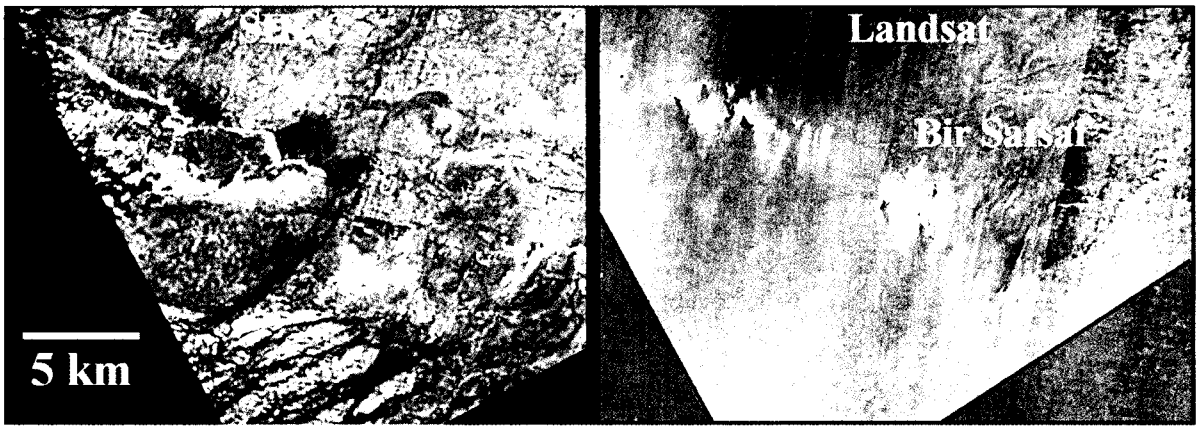

Figure 3. Shuttle Imaging Radar C (SIR-C) L-band radar image and matching Landsat image of the Bir Safsaf region of southern Egypt. The digitate dark pattern at lower center of the radar scene is part of the pre-Nile trans-African drainage network, buried beneath a sand sheet (courtesy T. Maxwell).

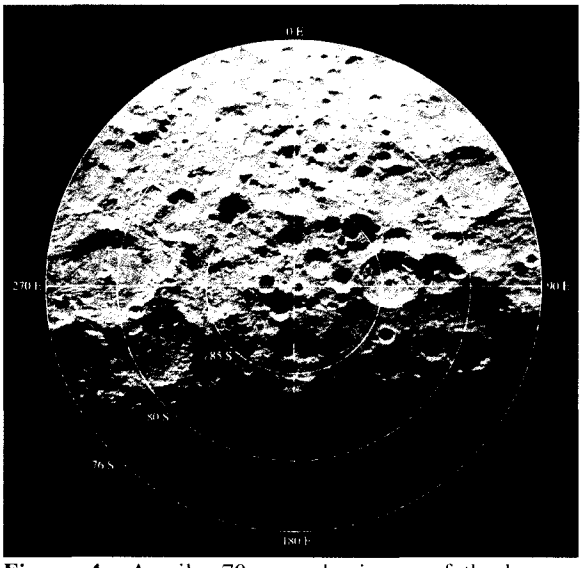

Figure 4. Arecibo 70-cm radar image of the lunar south pole. Image resolution 300 m per pixel [13].

Beyond the qualitative examples above, we are pursuing studies that validate our quantitative approach to Mars polarimetric radar studies. For this work, the NASA/JPL AIRSAR P-band system (68 cm wavelength) is an ideal test-bed. The fully polarimetric AIRSAR data permit synthesis of backscatter coefficient values for any desired transmit/receive polarization state. We also have a considerable base of surface roughness information for terrestrial test sites on centimeter-meter scales, and new work is augmenting these topographic data with ground-penetrating radar surveys of the near-surface structure [14, 15].

Figure 5 shows an AIRSAR color-composite image of the Kilauea Volcano summit region, Hawaii. Our interest in this area is P-band radar penetration of ash deposits erupted during occasional explosive events from the Kilaeau caldera. These deposits form a thin mantle in some areas, while close to the caldera they can be 10's of meters in total accumulated depth. The surface expression of the ash can be quite smooth (Figure 6). Ongoing work is focused on relating the observed P-band radar echoes to sub-surface interfaces revealed by GPR transects of the ash (Figure 7). These GPR data clearly show dielectric horizons within the 1-2 m penetration range of the AIRSAR signals.

Figure 5. AIRSAR C, L, P-band (R,G,B) color composite image of the Kilauea Volcano caldera and Ka'u desert; HV polarization.

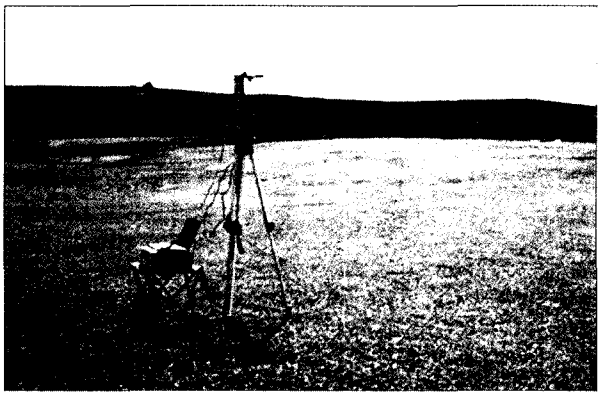

Figure 6. Ash deposit surface at Kilauea. The tripod supports a laser micro-topography mapper (sub-cm accuracy).

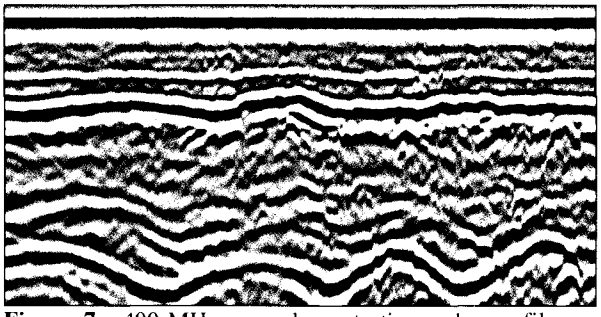

Figure 7. 400-MHz ground-penetrating radar profile through the ash shown in Figure 6. Vertical scale is ~2 m, horizontal scale ~200 m. The two major interfaces likely reflect cemented horizons between ash eruptions.

4. A P-BAND RADAR for MARS

The P-band imaging radar system designed for Eagle addresses a number of challenges to achieve high science return within a tightly constrained budget.

Design and cost drivers were identified based on experience with several spaceborne radar instruments (e.g. the SIR series, Magellan, Cassini, MARSIS). These include the complexity of the system (number of operational modes), antenna type, and system heritage. The system design uses a low-power, low-mass SAR system for which the data rate has been minimized. The body-fixed radar antenna is pointed sideways at the ground, perpendicular to the satellite velocity vector, with a 68-km wide footprint at an incidence angle of 40°. The radar system sends out pulses that illuminate this entire swath (Figure 8). Radar echoes are collected for only a portion of the illuminated swath, at most 28 km.

To simplify operations, the system has just four science modes (Table 1). An independent transmitter is included for each polarization to allow graceful degradation if one transmitter fails. Repeat-pass interferometry data is collected in the VV mapping mode. Calibration data will be collected as part of each data-taking sequence (including a receive-only sequence). Most science data would be collected in the VV or HH mapping modes. The only difference between HH and VV mapping modes is the selection of which transmitter to enable.

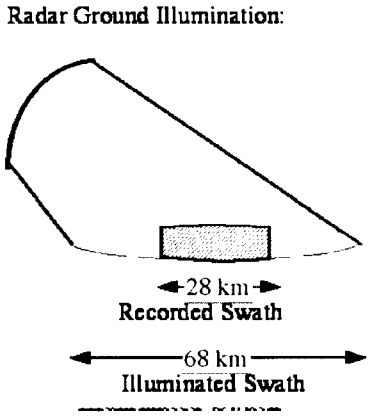

Figure 8. The radar imaging geometry is side-looking, perpendicular to the satellite velocity vector. The recorded swath is located near the center of the illuminated swath.

The SAR parameters and performance are summarized in Table 2. The radar draws 174 W when operating, and has sufficient bandwidth (2.5 and 7.5 MHz) to meet the ground-range spatial resolution requirements. The transmitted pulse length is 40 or 100 ms, and the pulse repetition frequency (PRF) is held constant at either

Table 1. Radar system operating modes.

Radar Mode	Function
VV Mapping	Mapping at VV polarization
HH Mapping	Mapping at HH polarization
Hi-res	30 m resolution
Nadir-sounding	Collect data in nadir-pointing configuration
Standby	Reduce power consumption when not collecting data
Power Off	Minimize power consumption during cruise phase/orbit insertion and aerobraking

1330 or 1444 Hz (dependent on the orbit altitude). The noise floor is better than –35 dB noise-equivalent ×° in the 100 m resolution mode. [Note: the radar design has an additional 5 dB margin built in.] The 6 m diameter antenna has a fixed look angle, so the field of view covered by the illuminated beam is 35-39° (off-nadir), corresponding to aggregate incidence angles of 38-42° at the surface. With this FOV the illuminated swath on the ground is ~68 km wide.

Table 2. Radar performance characteristics.

Radar Parameter	Mapping modes	Hi-res mode	Nadir mode
Center Frequency (MHz)	475	475	475
Bandwidth (MHz)	2.5	7.5	2.5
Peak Transmit Power (W)	500	500	500
Pulse Width (μsec)	40	100	30
Polarization	VV or HH	VV or HH	VV
Ground Resolution (m)	100	30	34 (range only)
Ground Swath (km)	28	28	8 x 8
Field of View (Look Angles in °)	35 to 39	35 to 39	-2 to +2
Noise Equivalent Sigma0 (dB)	-40 to -35	-33 to -30	-60
Worst Case Ambiguity (dB)	-19	-19	N/A
PRF (Hz)	1330/1444	1444	1330
DC Power Draw (W)	174	185	100
Data Format	2-bit BFPQ x4 pre-sum	2-bit BFPQ x4 pre-sum	2-bit BFPQ
Peak Buffered Data Rate (Mbps)	0.8	2	.75

The mapping strategy is to collect data for half an orbit, starting over one pole and finishing at the other. The position of the recorded swath is adjusted throughout each data-take in a preset sequence by varying the start and stop time of the recorded data window. One change

in PRF is made during each mapping pass (to maintain azimuth ambiguity levels at < -19 dB as the spacecraft altitude changes.) All other radar parameters (bandwidth, transmit power, gain, pulse length, data compression) are held constant throughout the data-take. This approach has flexibility to handle the changes in range due to topographic and orbit altitude variations. By changing the data window position in 0.75 km increments, for example, when the terrain height changes by more than 1 km, the recorded swath can be kept in the center of the antenna footprint.

To reduce the data volume by up to 30%, while preserving sufficient overlap between data from successive orbits, the width of the recorded data window is varied. Initially set at 8 km, it is progressively increased to 28 km at the equator, then decreased again to 8 km. These data segments, or lunes, are similar in shape to the outside edge of an orange segment. The peak (instantaneous) data rate of 0.8 Mbps corresponds to the widest section of a lune, collected in the vicinity of the Martian equator. The total data collected for a lune is ~2.0 Gbits.

The 6 m radar antenna, combined with a PRF of 1330 or 1444 Hz, allows along-track (or azimuth) resolution of ~3m. This resolution exceeds that required for the science data (100 m), permitting a reduced data rate. To achieve this, we incorporate an azimuth prefilter, which extracts the central 1/4 of the available Doppler bandwidth and reduces the data volume by a factor of 4. This approach is preferred over burst mode operation (after Magellan) since it simplifies the collection of repeat-pass interferometry data. A further factor of 4 reduction in data volume is achieved using the (8, 2) Block Floating Point Quantization (BFPQ) employed on Magellan.

Antenna: The SAR uses a low mass deployable antenna ~6 m in diameter. An offset feed configuration was selected to best fit the spacecraft/launch vehicle configuration and maximize gain (Figure 9). This is a fully offset deployable mesh reflector antenna assembly that includes a support boom and a microstrip patch feed: a proven, low risk technical approach that provides high efficiency and excellent antenna performance (Table 3). This antenna supports both SAR data collection and X-band telecom by using a dual-polarized microstrip patch feed at P-band and a horn feed at X-band. The 6-m offset reflector has a 3 m focal length (F/D=0.5) and height offset of 0.5 m. The feed is tilted by 60.5° relative to the reflector axis and requires a beamwidth of 85.1°, satisfied by a 2x2 microstrip patch array (Figure 9b). The panel is constructed of a lightweight honeycomb sandwich structure. A small horn in the center of the patch array serves as the X-Band feed. Antenna performance is summarized in Table 3.

Table 3. High-gain antenna performance for both radar operations and telecom.

	P-Band Radar	X-Band Telecom
Frequency	475 MHz	8.5 GHz Tx 7.1 GHz Rx
Bandwidth	2.5/7.5 MHz	~1 MHz
Polarization	Dual-linear (H & V)	Single-pol circular
El Beamwidth	~ 7.5°	~ 0.5°
Az Beamwidth	~ 7.5°	~ 0.5°
Gain	27 dB	50 dB
El Sidelobes	-20 dB	-20 dB
Az Sidelobes	-20 dB	-20 dB
Cross Polarization	< -25 dB	Circular

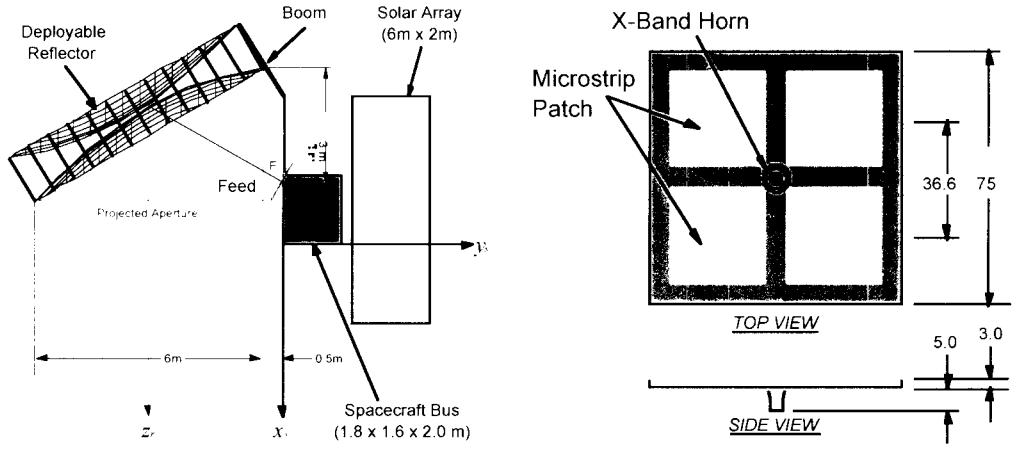

(a) Baseline reflector configuration (b) Baseline feed design

Figure 9. The mission antenna configuration is a low-mass offset-fed parabolic reflector (units in meters) with a dual-polarized microstrip patch feed (units in centimeters) at P-Band for SAR operations and a horn feed for X-band telecom.

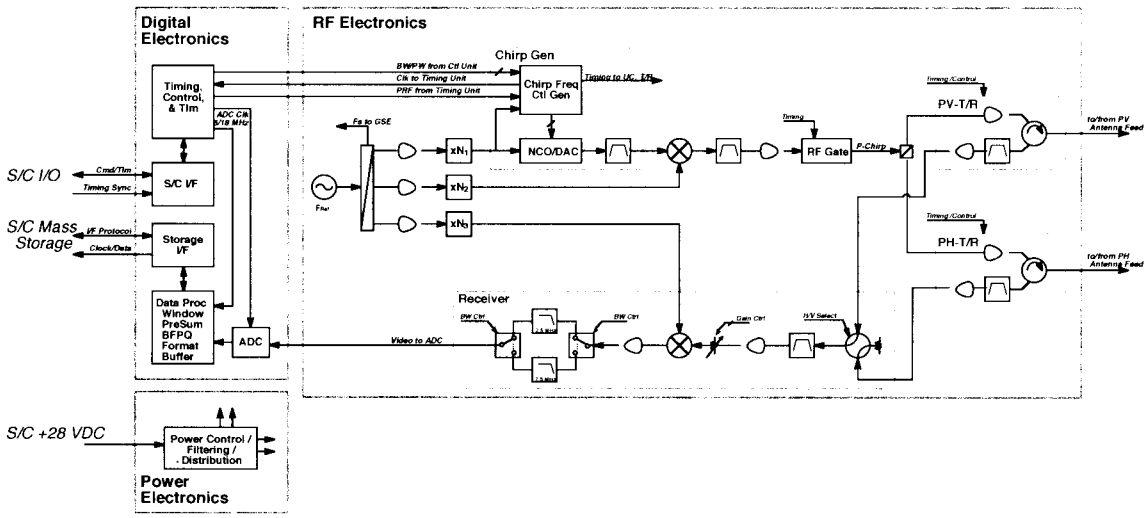

Figure 10. Radar instrument block diagram.

The radar electronics are a low-mass, low-power design (Figure 10). A timing and control unit triggers all radar operations and a power electronics unit conditions and routes power to each radar assembly. A stable local oscillator/frequency multiplier assembly provides constant frequency outputs and an initial carrier for the transmitted pulse, and a chirp generator modulates the 40 or 100 μs, 2.5 or 7.5 MHz chirp onto this carrier.

Table 4. Instrument performance characteristics.

Parameter	Value
Imaging Geometry	a) Look angle 37° (off-nadir) b) Nadir-pointing
Wavelength	63 cm
Polarizations	VV or HH
Number of science modes	4
Spatial resolution	30/100 m
Swath width	8 – 28 km
Mass (with contingency)	76.9 (20.8) kg
Stowed antenna dimensions	176 x 33 x 33 cm
Electronics box dimensions	20 x 30 x 40 cm
Average Power needs CBE (contingency)	174 (46) W
Buffered data rates	0.75 to 2 Mbps
Pointing accuracy requirement	0.75 °
Absolute calibration	± 3 dB
Relative calibration	± 1.5 dB

After upconversion to P-Band, this chirp signal is amplified by the 500-W solid-state amplifier in the P-Band Transmit Receive (T/R) subassembly. Either the H-Pol or the V-Pol T/R subassembly is enabled to direct the signal to the H or V polarized antenna feed. The return echoes are directed through the same feed to the receiver where a polarization switch routes the signal from the selected feed for filtering and downconversion to video frequency. The video signals are then passed to the digital subsystem for Analog-to-Digital conversion, pre-filtering and BFPQ formatting. This radar data stream is buffered, then forwarded to the onboard disk storage for subsequent transmission to Earth. A performance summary for the radar instrument is given in Table 4.

5. Mars Mission Operations

The Eagle mission design is very similar to that of Odyssey, and launches on a Delta 2925. After orbit insertion and aerobraking at Mars, the mapping orbit (Table 5) is achieved. The mission timeline (Figure 11) is designed to meet the science objectives in the shortest possible time. The design provides a 20-day launch period, an 11-month cruise, and a 24-day arrival period. Mars Orbit Insertion is performed with a single 15-min burn to capture into an elliptical orbit. Aerobraking over 2.5 months reduces the orbit period. Deployment of the high gain antenna (HGA) occurs after aerobraking and prior to conjunction.

The circumference at the equator of Mars is about 21350 km. For a 28 km swath width at the equator with no overlap we must acquire 760 lunes (with a 12% overlap this becomes 850). The orbit selected provides the opportunity to observe all parts of Mars every 10 weeks. Mapping over two of these cycles (140 days) allows time to eliminate data gaps. Therefore, to produce global mosaics mapping proceeds at a rate of on average 850 divided by 140, or just over 6 lunes/day.

Global mapping in VV and HH polarization is performed in two 20-week cycles (Fig. 11). A 12-week period follows to acquire near-nadir, high resolution, and repeat-pass data. Also shown in the figure is a detailed accounting of 50 hours of mapping activities. Each day consists of 16 hours of data taking and 8 hours of DSN downlink. A key feature of this mission is the dual use of the 6-m antenna for both mapping and downlink, enabling the return of the large data volume and minimizing total mission duration.

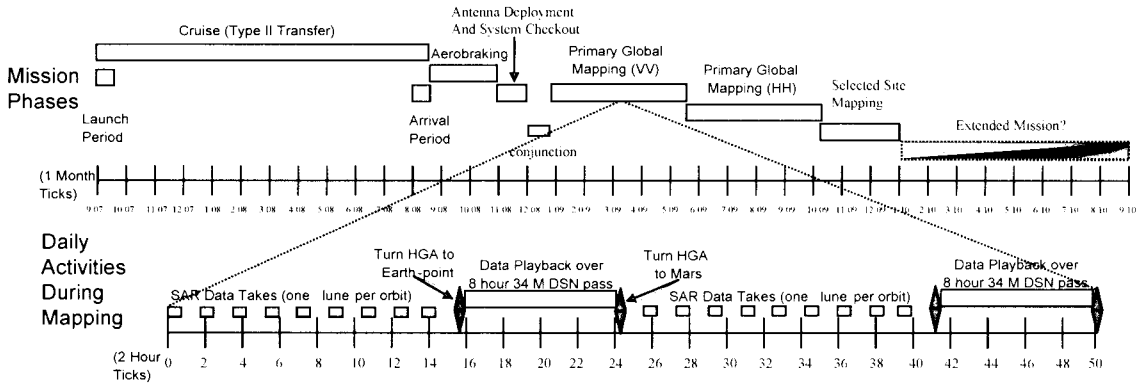

Figure 11. The Mission timeline is designed to maximize the science return at Mars while minimizing the length of the observation period

Table 5. Eagle orbit summary.

Orbit Element	Characteristic
Mapping Orbit Altitude	240 × 320 km Frozen
Mapping Orbit Inclination	92.8 deg
Mapping Orbit Node Local Time	3:30 – 5:00 pm
Start of mapping cycle	January 2009
VV and HH mapping cycle duration	40 weeks
Targeted mapping cycle duration	12 weeks

CONCLUSIONS

We have described a P-Band SAR system capable of penetrating the dust that covers much of the surface of Mars to reveal hidden geologic and hydrologic features. The data collection and return strategy is capable of global mapping of Mars in under 12 months.

REFERENCES

[1] Christensen, P.R., 1986. Regional dust deposits on Mars: Physical properties, age, and history: J. Geophys. Res., v. 91, no. B3, p. 3533-3545.

[2] Harmon, J.K., Arvidson, R.E., Guinness, E.A., Campbell, B.A. and Slade, M.A. 1999. Mars mapping with delay-Doppler radar. J. Geophys. Res., 104, 14,065-14,089.

[3] Simpson, R.A., Harmon, J.K., Zisk, S.H., Thompson, T.W. and Muhleman, D.O., 1992. Radar determination of Mars surface properties. In: H. Kieffer, B. Jakosky, C. Snyder and M. Mathews (Editors), Mars. Tucson: Univ. of AZ Press.

[4] Carrier, W.D., Olhoeft, G.R. and Mendell, W., 1991. Physical properties of the lunar surface. In: Lunar Sourcebook. Cambridge Univ. Press, New York.

[5] McHugh, W.P., McCauley, J.F., Haynes, C.V., Breed, C.S. and Schaber, G.G. 1988. Paleorivers and geoarchaeology in the southern Egyptian Sahara. Geoarchaeology, 3, 1-40.

[6] Schaber, G.G., McCauley, J.F., Breed, C.S. and Olhoeft, G.R. 1986. Shuttle Imaging Radar: Physical controls on signal penetration and subsurface scattering in the eastern Sahara. IEEE Trans. Geosci. Rem. Sens., 24, 603-623.

[7] Boynton, W., et al. 2002, Distribution of hydrogen in the near-surface of Mars: Evidence for subsurface ice deposits, Science, 297, 81-85.

[8] Rignot, E. 1995. Backscatter model for the unusual radar properties of the Greenland ice sheet. J. Geophys. Res., 100, 9389-9400.

[9] Haldemann, A.F.C. and Muhleman, D.O. 1999. Circular-polarization radar properties of high-altitude ice: Western Kunlun Shan and central Andes. J. Geophys. Res., 104, 24,075-24,094.

[10] Harmon, J.K., Slade, M.A. and Hudson, R.S. 1992. Mars radar scattering: Arecibo/Goldstone results at 12.6- and 3.5-cm wavelengths. Icarus, 98, 240-253.

[11] Ostro, S.J. and al., e. 1992. Europa, Ganymede, and Callisto: New radar results from Arecibo and Goldstone. J. Geophys. Res., 97, 13,091-13,102.

[12] Harmon, J.K. et al. 1994. Radar mapping of Mercury's polar anomalies. Nature, 369, 213-215.

[13] Campbell, B.A., D. B. Campbell, J. F. Chandler, A. A. Hine, M. C. Nolan, and P. J. Perillat, Radar imaging of the lunar poles, *Nature*, 426, 137-138, 2003.

[14] Shepard, M.K., B.A. Campbell, M. Bulmer, T. Farr, L.R. Gaddis, and J. Plaut, The roughness of natural terrain: A planetary and remote sensing perspective, *Geophys. Res.*, 106, 32,777-32,795, 2001.

[15] Campbell, B.A., J.A. Grant, and T. Maxwell, Radar penetration in Mars analog environments (abstract), LPSC XXXIII, 2002.

BIOGRAPHIES

Dr. Bruce A. Campbell received his B.S. in Geophysics from Texas A&M University in 1986, and his Ph.D. in Geology and Geophysics from the University of Hawaii in 1991. He joined the staff of the Center for Earth and Planetary Studies in 1992. From 1996 to 1998, he was the Discipline Scientist for NASA's Planetary Instrument Definition and Development Program (PIDDP). He served as CEPS Chairman from 1998 until 2002. Dr. Campbell's research interests focus on applications of radar remote sensing to the understanding of volcanism, impact cratering, weathering, and other surficial processes on the terrestrial planets. He is a member of the Mars Reconnaissance Orbiter shallow radar sounder (SHARAD) science team.

Dr. Anthony Freeman is the manager of the Earth Science Programs Office at JPL. Until recently, he was manager of the Mission and Systems Architecture Section (311) at NASA's Jet Propulsion Laboratory, with responsibility for developing the architecture of all new JPL missions. He has been at JPL for 16 years. He worked in the Radar Science and Engineering Section (334) for 12 of those years, where he played a lead role in several ESSP mission proposals to NASA. Prior to that he worked on radar for 4.5 years at Marconi Research Center in the UK. He has a Ph. D. in Astrophysics and a bachelor's degree in mathematics from the University of Manchester in the UK where he was born and raised. Dr. Freeman was elected a Fellow of the IEEE in 2000 "for contributions to SAR data calibration and development of Synthetic Aperture Radar (SAR) image products," and is a professional member of the Remote Sensing Society. He has received several NASA Group Achievement Awards for his contributions and the NASA Exceptional Service Medal in 1995 for his role in the success of the SIR-C missions. He has published over 30 articles in refereed journals and made nearly 100 conference presentations. He has received several new technology innovation awards and holds two patents on SAR technology. He has presented many short courses to engineers, managers and scientists over the years, and currently teaches at Caltech, USC and UCLA. Dr. Freeman's research interests include the effects of Faraday rotation on Spaceborne SAR data and novel space mission architectures.

Robert Shotwell is the Project Systems Engineer for the Phoenix Mission to Mars, selected in the recent Mars Scout competition. Prior to that, Robert was selected into the JPL Mission Architects Development Program. He was responsible for the growth and development of a microspacecraft program at JPL, as well as Lead Systems Engineer for the Outer Planets missions studied during the Decadal Survey. Before joining Systems, he worked on the Mars Pathfinder Propulsion system, was responsible for delivery of the Xenon Feed System for Deep Space 1, assisted with the SRTM mission and spent two years in Advanced Propulsion R&D where he tested Hall thrusters, ion engines, arc jets, MPD thrusters and was responsible forcharacterizing the SIRTF vent nozzles and the Loral propulsion systems for Telstar-8. He has a bachelors in Aerospace Engineering (Magna Cum Laude) from Texas A&M University and a Masters in Astronautics from USC.

Mr. Michael K. Jones is currently the lead system engineer for advanced planning studies of the operations system that would support the Jupiter Icy Moons Orbiter Project, a nuclear powered spacecraft that would explore the three icy Galilean moons of Jupiter. He is also currently the End-to-end Information Systems Engineer for the CloudSat Project, an earth-orbiting spacecraft that will launch in 2005 and measure ice and water densities of Earth's clouds. He has 24 years of planetary and earth-orbiting flight project design and operations experience as a JPL system engineer. This experience includes advanced planning of project information system and mission operation system designs for missions, designing such systems for competitive mission proposals, task management and system engineering for information system technology development, detailed information system design for the Cassini Mission, operations of the Voyager Mission, system design of the Magellan Mission downlink operations, and

system engineering coordination of the implementation, integration, testing and training of the Magellan operations system. The Magellan Mission mapped the surface of Venus using synthetic aperture radar.

Louise Veilleux is a Principal Engineer in the Radar Science and Engineering Section at JPL. She is currently serving as Chief Engineer on the Ocean Surface Topography Mission Project that includes the Wide Swath Ocean Altimeter, a Ku-Band interferometric radar. She has been with JPL's Radar Section since 1983, where she developed spaceborne radar instruments for several missions including SIR-B/C and SRTM. Ms. Veilleux received the BSEE degree from the University of Maine at Orono in 1979, and the MS degree from MIT in 1982. She is a recipient of a NASA Exceptional Achievement Medal, a NASA Exceptional Service Medal, and several NASA Group Achievement Awards.